Fuel cell electric vehicle-to-grid

Experimental feasibility and operational performance as balancing power plant

Oldenbroek, V.; Hamoen, V.C.S.; Alva, S.; Robledo, C. B.; Verhoef, L. A.; van Wijk, A. J.M.

DOI
10.1002/fuce.201700192

Publication date
2018

Document Version
Final published version

Published in
Fuel Cells

DOI: 10.1002/fuce.201700192

Fuel Cell Electric Vehicle-to-Grid: Experimental Feasibility and Operational Performance as Balancing Power Plant▲

V. Oldenbroek[1]*, V. Hamoen[1], S. Alva[1], C. B. Robledo[1], L. A. Verhoef[2], A. J. M. van Wijk[1]

[1] Delft University of Technology, Department of Process and Energy – Energy Technology Section, Leeghwaterstraat 39, 2628 CB Delft, The Netherlands

[2] Delft University of Technology, Green Office, van den Broekweg 2, 2628CS Delft, The Netherlands

Received November 09, 2017; accepted June 07, 2018; published online July 4, 2018

Abstract

The world's future energy supply will include intermittent renewable sources, such as solar and wind power. To guarantee reliability of supply, fast-reacting, dispatchable and renewable back-up power plants are required. One promising alternative is parked and grid-connected hydrogen-powered fuel cell electric vehicles (FCEVs) in ''Vehicle-to-Grid'' systems. We modified a commercial FCEV and installed an external 9.5 kW three-phase alternating current (AC) grid connection. Our experimental verification of this set-up shows that FCEVs can be used for mobility as well as generating power when parked. Our experimental results demonstrate that present-day grid-connected FCEVs can respond to high load gradients in the range of –760 % s^{-1} to + 730 % s^{-1}, due to the parallel connection of the high voltage battery and the fuel cell stack. Virtual power plants composed of multiple grid-connected FCEVs could perform higher power gradients than existing fast-reacting thermal power plants with typical power gradients of 1.67 % s^{-1}. Hydrogen consumption in 9.5 kW AC grid-connected mode was 0.55 kg h^{-1}, resulting in a Tank-To-Grid-AC efficiency of 43% on a higher heating value basis (51 % on a lower heating value basis). Direct current to alternating current efficiency was 95 %.

Keywords: Balancing Power Plant, Efficiency, Electrical Energy Services, Fuel Cell Electric Vehicle (FCEV), Hydrogen, PEM Fuel Cell System, Spinning Reserve, Tank-To-Grid (TTG), Vehicle-to-Grid (V2G)

1 Introduction

As shares of intermittent renewable energy sources increase [1], stationary back-up power plants [1–5] will face even lower utilization factors in coming years and require expensive back-up power [1, 2, 6–8]. Passenger cars also face low utilization factors and could be put to better use while parked. On average, passenger cars drive 12,000 km per year at an average annual speed of 45 km h^{-1} [9]. They are parked 97 % of the time. One promising alternative to stationary back-up power plants is parked and grid-connected electric vehicles (EVs). EVs are able to provide power to the grid while parked, which is known as a "Vehicle-to-Grid" (V2G) system [10, 11]. The combined installed power capacity of passenger cars is enormous [12]. Every year, more than 80 million new cars are sold worldwide. Van Wijk et al. [12] multiplied the number of cars sold annually by 100 kW of future installed electric power per car and calculated that 8,000 GW of power capacity in cars would be sold each year. The installed power plant capacity worldwide is only around 5,000 GW [12].

There are three types of EVs that are suitable for delivering renewable power while parked: battery electric vehicles (BEVs), plug-in hybrid electric vehicles (PHEVs) and fuel cell electric vehicles (FCEVs) [10, 11]. This article focuses on FCEVs for V2G use. Commercially available FCEVs use proton exchange membrane fuel cells (PEMFCs) to convert hydrogen

▲ *Paper presented at the 6th EUROPEAN PEFC & ELECTROLYZER Forum (EFCF2017), July 4–7, 2017 held in Lucerne, Switzerland. Organized by the European Fuel Cells Forum – www.efcf.com*

[*] *Corresponding author: v.d.w.m.oldenbroek@tudelft.nl*

into electricity and have a high voltage (HV) [13] battery connected in parallel [14–16]. The battery is used for regenerative braking and provides additional power for acceleration. This combination of FC and HV battery is capable of delivering almost every kind of electrical energy service [17], from balancing to emergency power back-up [18], primary reserve [10, 19, 20] or reconverting hydrogen from seasonal hydrogen energy storage in underground salt caverns [18]. Hundreds of grid-connected FCEVs sitting in parking lots could function as local power plants [21] and balance entire cities and countries [22], resulting in cost-effective balancing power for intermittent power sources [23].

Brauner et al. [2] identified the following operational requirements for balancing power plants in the future, once high shares of intermittent renewables have been achieved, and particularly in cases where large-scale pumped storage is limited or unavailable:

(i) ability to perform high power gradients (≥ 0.05 % s^{-1} of all plants in the grid combined);
(ii) ability to be operated at low minimal generation (e.g., 15–20 % instead of 40 %);
(iii) high efficiency under partial load as well as nominal load (e.g., 25 % instead of 50 % partial load);
(iv) high number of start-ups and shutdowns (e.g., 0.5 start-ups and shutdowns per day instead of 0.25 start-ups and shutdowns per day);
(v) ability to schedule cars in the face of an insecure day ahead energy prognosis.

Brauner et al. stated [2] that, for a load gradient of 15 GW h^{-1} in the grid, approximately 25 GW of flexible power plants with 0.0167 % s^{-1} of power capacity must be available for the German electricity system in 2020. However, the available capacity could be reduced to 8 GW, if an ability of 0.05 % s^{-1} could be achieved. Aeroderivative open-cycle gas turbines and gas engines can reach 1.67 % s^{-1} under hot start conditions [24–27], reducing the available capacity to 0.25 GW – this amount corresponds to 25,000 cars at a rated capacity of 10 kW. Increasing the ability to perform high power gradients reduces the number of power plants in hot standby and economizes energy [2].

Therefore, the question arises as to whether grid connected FCEVs can fulfil these requirements. In order to gain insight and answers to this question, in this study, we analyzed the feasibility and operational performance of a commercial Hyundai ix35 FCEV [14] modified for V2G purposes combined with a 9.5 kW three-phase AC (alternating current) grid connection [28].

2 Experimental

A number of FCEV manufacturers [15, 29, 30] are developing FCEVs capable of providing power to electric appliances (Vehicle-to-Load, V2L), small grids or homes (Vehicle-to-Home, V2H) [31], although none claim to have connected a FCEV to a low-voltage national AC grid. At the Car as Power Plant project at The Green Village in The Netherlands, we modified a Hyundai ix35 FCEV to include a power outlet plug and designed a discharge unit which connects the car to the Dutch national electricity grid (see Figure 1). We have conducted experiments with the car in idling mode (simulated "spinning reserve" mode) since January 2016. Since July 2016, we have carried out further experiments with the car connected to the grid and delivering 9.5 kW three-phase AC power. We measured the performance of the FCEV in both V2G and idling mode, by analyzing the data obtained from various sensors, the discharge unit, and a data logger installed in the car in MATLAB®.

The experimental set-up consisted of three main components:

(i) a modified commercially available Hyundai ix35 FCEV [14, 32] with a V2G DC (Direct Current) outlet plug;
(ii) a Vehicle-to-Grid DC-AC discharge unit (V2G-DCAC) that converts DC power in the range of 300–400 V re-

Fig. 1 Experimental Fuel Cell Electric Vehicle-to-Grid (FCEV2G) set-up at The Green Village, Delft University of Technology, Delft, The Netherlands.

ceived from the FCEV into three-phase AC power at 380 V. The power discharge setting can be manually defined in the V2G-DCAC. DC switching safety and grounding was incorporated in the V2G-DCAC unit;

(iii) a three-phase 380 V AC grid connection including fuses and kWh meter.

2.1 Modified Hyundai ix35 FCEV for V2G Purposes

The modified Hyundai ix35 FCEV [14, 32, 33] has a 100 kW FC on board. In parallel, an HV battery with Bi-directional High-voltage DC-DC Converter (BHDC) is connected to the HV Junction Box (HVJB) [32, 33]. These components and connections are illustrated in Figure 2, which provides a scheme of the electrical architecture of the FCEV and the modifications. The battery has an energy capacity of 0.95 kWh and a maximum power output and input of 24 kW [33]. The electric motor that powers the wheels has a maximum power of 100 kW. The modifications consisted of an extra parallel connection in the HVJB for the DC outlet protected by a fuse [34] and activated by a relay switch [35]. We replaced the front bumper of the car with an adapted version to accommodate a Type 1 SAE J1772 [36] socket (see Figure 3). We used the socket for the DC connection to the V2G-DCAC discharge unit. Finally, we installed a software update for the car along with a dashboard activation button (see Figure 4) which also activates the Cold Shut Down procedure (CSD). We made no further adaptions to the FCEV. We maintained the vehicle's road access permit, in accordance with the requirements of the Dutch National Vehicle and Driving License Registration Authority (RDW). We logged the FC and HV battery operating voltage, current, and other power system-related parameters at a frequency of 1 to 5 Hz using a CAN bus data logger [37].

2.2 Vehicle-to-Grid DC-AC Discharge Unit

We fitted every component of the V2G-DCAC unit in a weather-proof enclosure, see Figure 5. Figure 6 illustrates the simplified electrical architecture of the V2G-DCAC and its main components. We connected the FCEV with the V2G-DCAC *via* a Type 1 socket and cable with plugs. We mounted a red-colored combined start-up and shutdown button which must be unlocked with a key. Cooling fins on the back of the enclosure enhanced possible heat dissipation for the three-phase grid-tie inverter [38]. The DC input and AC output voltages and currents were monitored every five minutes by the inverter and sent to an internet server. We programmed an Arduino shield [39] to establish a connection between the FCEV power outlet and the three-phase AC grid connection. The proximity detection and control pilot [36] and the lockable start button served as inputs for the control logic. The Arduino shield controlled the inverter, the DC relay, the three-phase switches, the relay and the Red-Blue-Green (RGB) LED strip indicating the current status. We installed a galvanic isolation transformer between the three-phase switches and the AC grid connection to prevent any stray voltage incidents [40].

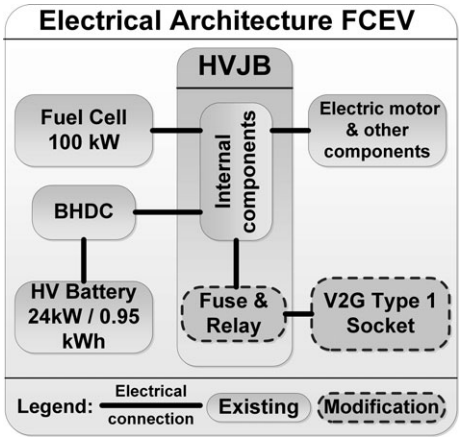

Fig. 2 Scheme of electrical architecture of the FCEV and V2G modification.

Fig. 3 V2G Type 1 Socket integrated in the front bumper.

Fig. 4 New dashboard V2G activation button also initiates Cold Shut Down.

2.3 AC Grid Connection

The three-phase 400 V AC grid connection included a C-characteristic circuit breaker, a class B ground fault circuit interrupter and an electricity meter.

2.4 Operation and Safety Fuel Cell Electric Vehicle-to-Grid

To commence delivering power to the grid, we start the inverter and synchronize with the electric grid upon activating

Fig. 5 V2G-DCAC unit connected to the FCEV.

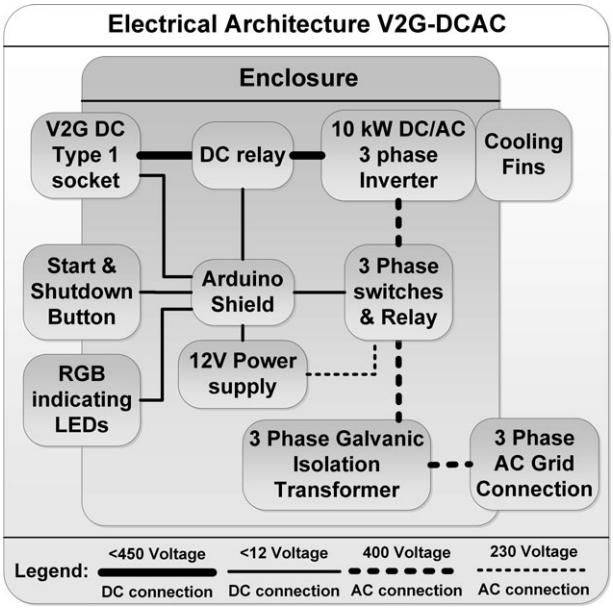

Fig. 6 Simplified electrical architecture of the V2G-DCAC connecting the FCEV to the AC grid.

the combined start-up and shutdown button. The inverter can be started up either before or after connecting the V2G cable and starting up the FCEV. To stop delivering power to the grid, we first switch off the AC load, in this case by switching off the inverter. The FCEV is programmed such that the V2G DC HV relay [35] opens the instant we switch the FCEV in V2G mode off or disconnect a load. This strict switch-off sequence could be avoided by applying DC arc suppression and contact protection [13, 41, 42].

2.5 Test Time, Start-up Time and Power Gradient Measurements

We drove the FCEV prior to performing each test and therefore only examined "warm starts" in V2G mode. During the V2G tests, we elected to start the FCEV up before applying any load (switching on the inverter), which enabled us to monitor load-switching behavior. The data logger in the FCEV was actively monitoring before any load was applied; therefore, the time during which the FCEV was switched on, t_{test}, was always somewhat longer than the grid connection time, t_{grid}. We calculated this as the difference between the end time and start time of the V2G tests, using Eq. (1):

$$t_{test} = t_{end} - t_{start} \tag{1}$$

This difference in test time with respect to the grid connected time is called the grid connect/disconnect time, $t_{GC/D}$. The grid connect/disconnect time was partly defined by the inverter start-up and grid frequency synchronization time (approximately 1 min) and the user's lingering time. We calculated this, using Eq. (2):

$$t_{GC/D} = t_{test} - t_{grid} \tag{2}$$

We calculated the gross electric power, $P_{component,e,gross}$, of the component, either the FC or the HV battery, by the product of the voltage, $U_{component}$, and gross current, $I_{component,gross}$, of the FC stack and battery every 0.2 s (5 Hz sample frequency), using Eq. (3):

$$P_{component,e,gross} = U_{component} \cdot I_{component,gross} \tag{3}$$

We measured the upward and downward power gradients of the FC and HV battery in V2G mode. The power gradients, $\Delta P\ \Delta t^{-1}$, are expressed in kW s^{-1} and were calculated, using Eq. (4):

$$\Delta P \Delta t^{-1} = \left(P_{component,e,gross@t+0.2s} - P_{component,e,gross@t}\right)/0.2\ \text{s} \tag{4}$$

The power gradients are also expressed in % change of maximum power per second % s^{-1}, negative for downward gradients and positive for upward gradients, as shown in Eq. (5):

$$\Delta P \Delta t^{-1} = \Delta P \Delta t^{-1}/P_{V2G\ DC\ max} \tag{5}$$

The maximum V2G DC power, $P_{V2G\ DC\ max}$ was 10 kW. Electric powers were measured every 0.2 s (5 Hz sample frequency).

2.6 Efficiency FCEV2G and Hydrogen Consumption

The efficiency of the combined FCEV and V2G-DCAC system is called Tank-To-Grid AC (T2G-AC) efficiency, $\eta_{TTG\text{-}AC}$, was calculated, using Eq. (6):

$$\eta_{T2G-AC} = (E_{AC} + \Delta E_{HV\ Bat})/E_{H_2} \tag{6}$$

where E_{AC} is the three-phase AC electrical energy delivery to the grid. $\Delta E_{HV\ Bat}$ is the difference in HV battery energy. E_{H_2} is the hydrogen energy consumption, which we calculated, using Eq. (7):

$$E_{H_2} = \Delta m_{H_2} \cdot \text{HHV} \tag{7}$$

based on the hydrogen Higher Heating Value HHV of 39.41 kWh kg^{-1}. We calculated the difference in HV battery energy by multiplying the difference in State Of Charge, ΔSOC, of the HV battery at the start and end of the test with the maximum energy capacity, $E_{HV\ Bat,\ max}$, of 0.95 kWh [33], using Eq. (8):

$$\Delta E_{HV\ Bat} = \Delta SOC \cdot E_{HV\ Bat,\ max} \tag{8}$$

This is a simplification of the HV battery characteristics since capacity according to C-rate and temperature [43, 44], but we were unable to take a more accurate approach, due to lack of battery-specific information. Therefore, we included the charging and discharging efficiency of the HV battery in the $\eta_{T2G\text{-}AC}$, as well as the BHDC conversion efficiency. We calculated the hydrogen consumption, Δm_{H_2}, by the difference in hydrogen density at the start and end of the test, ρ_{start} and ρ_{end}, multiplied by the fixed volume capacity of 0.144 m^3 [14] of the hydrogen tanks, V_{tanks}, on board, as shown in Eq. (9):

$$\Delta m_{H2} = V_{tanks} \cdot \left(\rho_{start}\left[p_{tanks,start}, T_{tanks,start}\right] - \rho_{end}\left[p_{tanks,end}, T_{tanks,end}\right]\right) \tag{9}$$

We calculated hydrogen density using measured hydrogen tank pressures, $p_{tanks,start}$ and $p_{tanks,end}$, and temperatures, $T_{tanks,start}$ and $T_{tanks,end}$, at the start and end of the test and REFPROP software [45]. We calculated inverter efficiency, η_{DCAC}, by dividing the delivered AC Energy, E_{AC}, by the incoming DC energy, E_{DC}, as shown in Eq. (10):

$$\eta_{DCAC} = E_{AC}/E_{DC} \tag{10}$$

We calculated the Tank-to-Grid DC efficiency, $\eta_{T2G\text{-}DC}$, which may be considered an approximation of the efficiency of the FC and HV Battery system, as per Eq. (11):

$$\eta_{T2G-DC} = \eta_{T2G-AC}/\eta_{DCAC} \tag{11}$$

We calculated the hydrogen consumption rate, $\Delta m_{H_2}\Delta t^{-1}$, by dividing the hydrogen consumption obtained in Eq. (9) by the duration of the test obtained in Eq. (1), as shown in Eq. (12):

$$\Delta m_{H_2}\Delta t^{-1} = \Delta m_{H_2}/t_{test} \tag{12}$$

We obtained the hydrogen consumption in "spinning reserve" mode [19], by keeping the FCEV in idling mode. In the spinning reserve case, no power was delivered to either the grid or the electric motor. The cabin heating and cooling, entertainment, navigation devices and lighting were all switched off. During the V2G tests, in addition to delivering power to the grid, the FC and HV battery also deliver power to the on-board devices which cannot be switched off manually, such as FC auxiliary components and instruments. All of the calculated efficiencies include any hydrogen and HV battery energy use by the FCEV during the grid connect/disconnect time.

3 Results and Discussion

3.1 Selection of Tests

We have carried out experiments with the car in idling mode (simulated "spinning reserve" mode), since January 2016. The duration of all "spinning reserve" tests was over nine hours, which equates to more than 0.35 kg of hydrogen consumption. Since July 2016, we conducted tests with the car connected to the grid and delivering three-phase 9.5 kW AC power. Although ambient conditions, such as temperature, wind speed, wind direction and solar radiation can all influence the cooling of the FC in 9.5 kW AC V2G mode, we did not investigate these factors for the purposes of this study. We selected tests based on similar coolant temperature and pump angular velocity behavior during the test. From the period between July 2016 and April 2017 (see Table 1), we selected eight V2G tests. The results of the V2G test conducted on February 13, 2017 are used as an illustrative example throughout this paper. Figure 7 shows the coolant temperature entering and leaving the radiator during the entire duration of the

Table 1 Maximum downward (↓) and upward (↑) power gradients of the FC and HV battery expressed in kW s^{-1} and % s^{-1} of maximum power output. Eight tests at 9.5 kW AC V2G conditions were performed and the values averaged.

#	Date / DD-MM-YY	t_{test} / h:mm	$t_{GC/D}$ / h:mm	$\downarrow \Delta P_{FC}\,\Delta t^{-1}$ / kW s^{-1}	$\downarrow \Delta P_{FC}\,\Delta t^{-1}$ / % s^{-1}	$\uparrow \Delta P_{FC}\,\Delta t^{-1}$ / kW s^{-1}	$\uparrow \Delta P_{FC}\,\Delta t^{-1}$ / % s^{-1}	$\downarrow \Delta P_{HV\ BAT}\,\Delta t^{-1}$ / kW s^{-1}	$\downarrow \Delta P_{HV\ BAT}\,\Delta t^{-1}$ / % s^{-1}	$\downarrow \Delta P_{HV\ BAT}\,\Delta t^{-1}$ / kW s^{-1}	$\downarrow \Delta P_{HV\ BAT}\,\Delta t^{-1}$ / % s^{-1}
1	15-08-16	5:51	0:05	–43	–430	73	730	–77	–770	32	320
2	16-08-16	7:05	0:05	–48	–480	72	720	–76	–760	30	300
3	13-02-17	6:05	0:05	–47	–470	73	730	–78	–780	51	510
4	14-02-17	5:59	0:05	–53	–530	72	720	–74	–740	38	380
5	15-02-17	6:06	0:04	–47	–470	73	730	–76	–760	41	410
6	17-02-17	6:06	0:04	–46	–460	74	740	–77	–770	57	570
7	11-04-17	5:56	0:03	–48	–480	73	730	–77	–770	54	540
8	12-04-17	6:26	0:19	–42	–420	72	720	–76	–760	39	390
Mean				–47	–470	73	730	–76	–760	43	430
Sample standard deviation				3	34	1	5	1	11	10	100

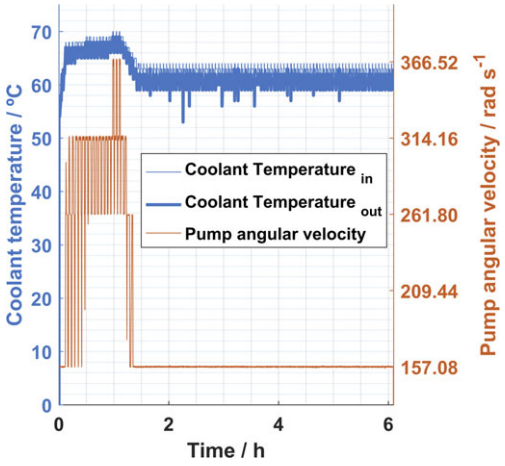

Fig. 7 Coolant temperatures and pump angular velocity at 9.5 kW AC V2G for the entire test duration of 6 h and 5 min on February 13, 2017.

February 13, 2017 test. Figure 8 shows a more detailed pattern for the period between 6,000 to 7,000 s for the coolant temperature difference and pump angular velocity. All eight V2G tests selected showed similar coolant temperature and pump angular velocity behavior and were characterized by a period of an elevated pump angular velocity of up to 367 rad s^{-1} and temperatures of up to 70 °C. Subsequently, the coolant temperatures and pump angular velocity decreased and stabilized to 60–64 °C and 157 rad s^{-1}, respectively. The exceptions were tests 5 and 8, in which there was a short period at the end of the test with elevated coolant pump angular velocity and temperatures.

3.2 Power Gradients

As an example, Figure 9 shows the gross electric power of the FC and HV battery over a period of 6 h and 5 min of the test on February 13, 2017. Figure 10 zooms into the period from 7,000–8,000 s (1 h 56 min to 2 h 13 min). Although the V2G AC output was fixed at a constant 9.5 kW, the FCEV

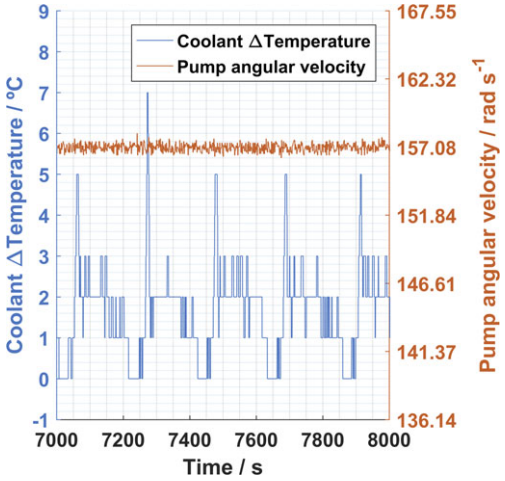

Fig. 8 Pump angular velocity and coolant temperature difference for the 7,000 to 8,000 s period for the test on February 13, 2017.

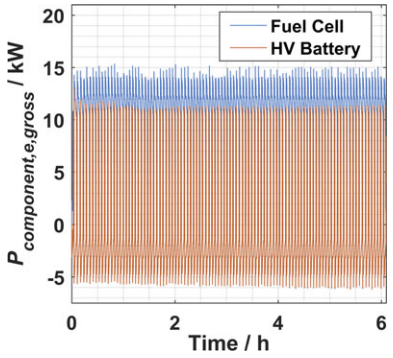

Fig. 9 FC and HV battery gross electrical power for the entire test duration of 6 h and 5 min on February 13, 2017.

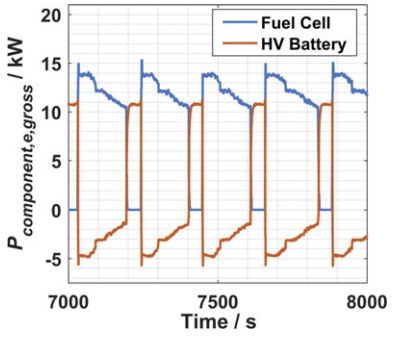

Fig. 10 FC and HV battery gross electrical power for the 7,000 to 8,000 s period for the test on February 13, 2017.

power management alternated between FC and HV battery power. The FC delivered power to the grid and recharged the HV battery. Figures 10 and 14 show that once the HV battery reached an *SOC* of 57.5 %, the FC was switched off and HV battery was discharged to an *SOC* of 42.5 %. The power management switched between FC and HV battery power. The executed V2G measurements can therefore also be used to analyze the power gradients of the FC and HV battery. The results of the power gradient analysis are set out in Figure 11, Figure 12 and Table 1. The mean maximum downward and upward power gradients of the FC were –47 kW s^{-1} (–470 % s^{-1}) and +73 kW s^{-1} (+730 % s^{-1}), respectively, at the sample frequency of 5 Hz. Sample standard deviations are 3 kW s^{-1} and

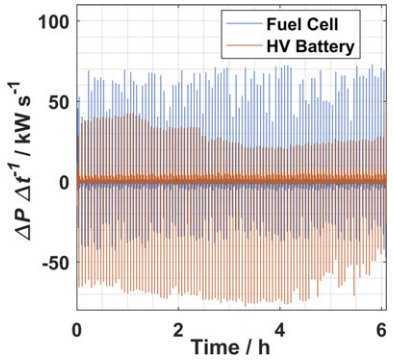

Fig. 11 Downward and upward power gradients of the FC and HV battery for the entire test duration of 6 h and 5 min on February 13, 2017.

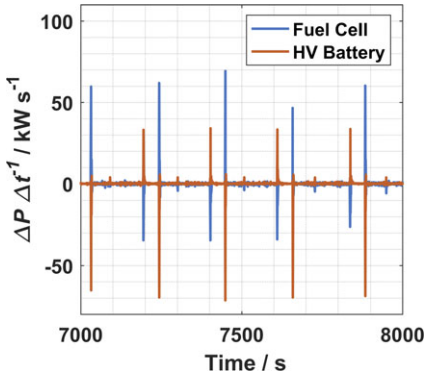

Fig. 12 Downward and upward power gradients of the FC and HV battery for the 7,000 to 8,000 s period for the test on February 13, 2017.

1 kW s^{-1}, respectively. The mean maximum downward and upward power gradients of the HV battery are –76 kW s^{-1} (–760 % s^{-1}) and +43 kW s^{-1} (+430 % s^{-1}), respectively, at the sample frequency of 5 Hz. Sample standard deviations are 1 kW s^{-1} and 10 kW s^{-1}, respectively. From these results, we concluded that the FC and the battery in particular are capable of responding many times faster than fast-reacting small-scale (<60 MW) aeroderivative open-cycle gas turbines and gas engines, with respective maximum values of 0.3 % s^{-1} for cold start and 1.67 % s^{-1} for hot start [24–27]. General Electric's LM6000 Hybrid Electric Gas Turbine combines a fast-reacting gas turbine with a large battery [46], which could be viewed as a forerunner of even faster-reacting combined FC battery balancing power plants. Combining the output of millions of grid connected FCEVs would create so-called Virtual Power Plants [47, 48] with – in theory – unlimited capacities and could balance entire cities [23] and national electricity grids. If the FC and HV battery power were combined, even higher absolute downward and upward power gradients of –123 kW s^{-1} and +116 kW s^{-1}, respectively, could be achieved (taking into account the 5 Hz sample frequency). Relative power gradients in % s^{-1} can be tailored to the requirements of energy services [17, 19, 20] by selecting different FC and battery power capacities.

The impact of additional V2G load ramps and different power management strategies on the durability of the combined FC and battery system is yet to be quantified. Many studies focus primarily on V2G impact [49–54] on batteries in BEVs, but little is known about how the V2G mode will impact FC degradation in FCEVs.

It is estimated that, during a vehicle's lifetime, the powertrain faces 300,000 full load power gradients (0–100% rated power) [55]. Several studies show that start-ups/shutdowns and high load cycles can reduce FC durability [56, 57]. In the V2G mode experiments performed in this study, load ramps were limited to approximately 10 kW, corresponding to only 10% rated power of the FC in the car, which is relatively small in comparison to the full load ramps in driving mode.

Approximately 38,500 start-up/shutdown cycles take place during the 5,500 h life of an FCEV [55]. If FCEVs were never switched off and instead continuously used for either driving or V2G energy services, start-up/shutdowns would be eliminated. Additional degradation due to V2G load cycles (less than 10 % rated power) could possibly be compensated for by a reduction in start-ups/shutdowns. Furthermore, a smarter power management system of both FC and HV battery could be applied or ultra-capacitors introduced [58].

3.3 Start-up Time

FCEVs are already capable of cold start-up time to 50 % of their rated power within ten seconds at an ambient temperature of 20 °C and within 20 s at –20 °C [59]. In our V2G tests, using the modified Hyundai ix35, we measured cold start-up times of less than 5 s at ambient temperatures. Driving to cruising speed can already be achieved within 11 s at –20 °C [60], which is comparable to V2G power of 10 kW (10 % of the rated FC power). The newer model Toyota Mirai FCEV is even able to provide full stack power of 114 kW at –30 °C within 70 s [15].

In conclusion, today's FCEVs have extremely fast start-up times for providing V2G services to full rated power even at very low ambient temperatures. If FCEVs were never switched off and continuously used for either driving or V2G energy services, cold start-up temperature could even become irrelevant.

As described in Section 2, the way we started our V2G tests incurred additional start-up and grid frequency synchronization time. To further reduce grid connection times, the inverter could also be switched on before connecting and turning on the FCEV, eliminating additional start-up and grid frequency synchronization time from the inverter. Moreover, inductive discharging instead of conductive discharging (by cable) could reduce any further grid connection time [61–64], and likewise specialized FCEV V2G inverters with reduced reaction time and tailored Maximum Power Point Tracking or combining the V2G inverter with solar photo-voltaic inverters [65].

3.4 System Efficiencies & Hydrogen Consumption in V2G Mode

The hydrogen content in the two tanks and HV battery state of charge during the illustrative test on February 13, 2017 are shown in Figure 13, Figure 14 and further V2G test results are presented in Table 2. Fluctuations and 1 °C accuracy of the tank temperature sensors have an impact on the hydrogen density calculations (Eq. (9)), therefore we applied a 90-second moving average to the hydrogen mass calculation and used this in our hydrogen consumption calculations.

The average V2G test duration was approximately six hours with a mean hydrogen consumption of 3.44 kg and consumption rate of 0.55 kg h^{-1} per test. The maximum capacity of the hydrogen tank is 5.6 kg, with a minimum operating pressure of approximately 2.5 MPa; 5 kg for V2G energy services and the remaining hydrogen is enough to fulfill average European daily driving [9] requirements and reach a hydrogen filling station before using the car in V2G mode again. At a consumption rate of 0.55 kg h^{-1}, approximately nine hours of

Table 2 Test durations with hydrogen consumption rates and corresponding AC and DC system efficiencies.

#	Date / DD-MM-YY	t_{test} / h:mm	$t_{GC/D}$ / h:mm	Δm_{H_2} / kg	$\Delta m\ \Delta t^{-1}$ / kg h^{-1}	$\eta_{T2G\text{-}AC}$ / %	η_{DCAC} / %	$\eta_{T2G\text{-}DC}$ / %
1	15-08-16	5:51	0:05	3.28	0.56	42	95	44
2	16-08-16	7:05	0:05	3.96	0.56	42	95	45
3	13-02-17	6:05	0:05	3.34	0.55	43	95	45
4	14-02-17	5:59	0:05	3.33	0.56	42	95	45
5	15-02-17	6:06	0:04	3.39	0.56	43	95	45
6	17-02-17	6:06	0:04	3.38	0.55	43	95	46
7	11-04-17	5:56	0:03	3.33	0.56	43	95	46
8	12-04-17	6:26	0:19	3.51	0.54	42	95	44
Mean				3.44	0.55	43	95	45
Sample standard deviation				0.22	0.01	1	0	1

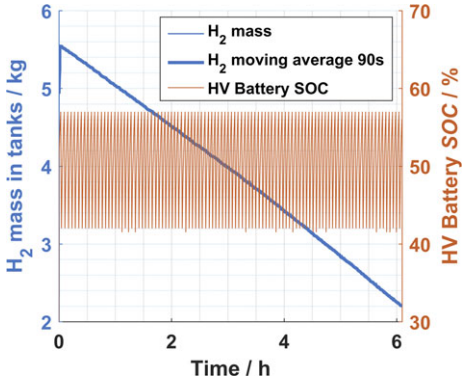

Fig. 13 Hydrogen mass in tanks and HV battery state of charge (SOC) cycling for the entire test duration of 6 h and 5 min on February 13, 2017.

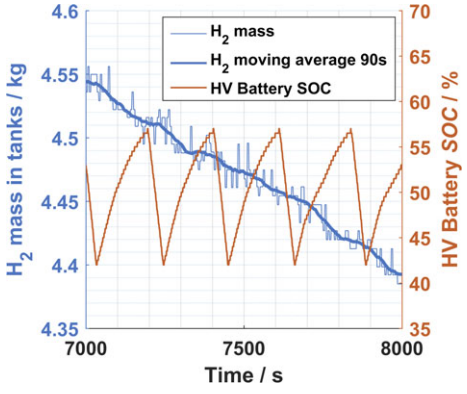

Fig. 14 Hydrogen mass in tanks and HV battery state of charge (SOC) cycling for the 7,000 to 8,000 s period for the test on February 13, 2017.

AC power can be delivered to the grid on a full tank, resulting in 86 kWh. The mean $\eta_{T2G\text{-}AC}$, η_{DCAC} and $\eta_{T2G\text{-}DC}$ efficiencies were 43 % (51 % on an LHV basis), 95 % and 45 % (53 % on an LHV basis), respectively. The values of the efficiencies we calculated were consistent throughout all the tests.

As discussed in Section 3.2, $\eta_{T2G\text{-}DC}$ is an approximate value of the efficiency of the FC and HV battery system. $\eta_{T2G\text{-}DC}$ is in line with the 43–51 % FC system efficiencies of FCEVs in driving mode at 10–15 % rated power reported in literature [61, 66, 67]. The $\eta_{T2G\text{-}DC}$ of 45 % (53 % on an LHV basis) is close to the reported Hyundai ix35 FCEV FC system DC efficiency of 46.8% (55.3 % on an LHV basis) [68]. Current automotive FC stacks with power ranges of 80–100 kW, used as primary power source in FCEVs (not in a fuel cell range extender configuration), show highest FC system efficiency at 10–15 % rated power [66, 67]. Future automotive FC system developments aim for higher system efficiencies at even lower rated powers, as driving cycles, such as the NEDC, consist of high power frequencies below 10 % rated power [69, 70]. As mentioned in our introduction, the ability to operate balancing plants at low minimal generation (e.g., 15–20 % instead of 40 %) is important. In the performed V2G tests, the PEMFC was operating at only 10–15 % of its maximum generation capability, see Figure 10. It is possible for FCEVs to generate more power, although this would require a better understanding of the cooling capacity of the radiator [71] when parked and the maximum operating temperature of the PEMFC. Tests at different DC powers in the range of 0–10 kW done with the same set-up, show that 10 kW gives the highest V2G efficiency [72]. Conducting further tests at DC powers above 10 kW would provide full insight into the partial load and optimum V2G efficiency.

At relative low FC rated power of 10–15%, there is less water production on the cathode side of the FC. Depending on the amount of air supplied by the air-blower membrane humidification problems can occur with different and opposite effects [73]. A relative low air stoichiometry or sometimes called cathode stoichiometric factor, a relative low air flow rate is sent to the cathode channel and can result in a reduced removal of produced water [73,74]. Whereas at a high air stoichiometry, an increase of the water removal rate can result in membrane dehydration and higher membrane resistance [73]. When delivering 10 kW DC power to the grid and the fuel cell is producing power, see Figure 10, calculated average FC stack air stoichiometry is in the range of 2 up to 6 According to Heuer et al. [75] air stoichiometry above 3 can be considered high and increase the probability of accelerated degradation. Air stoichiometry at individual cells and within individual

cells [76] can differ significantly from the calculated FC stack average, for example for individual cells at the inlet there is a probability of too low membrane humidification, whereas for cells at the outlet there is a probability of too high membrane humidification [73–75].

Idling, low load and low current density are associated with cell potentials of 0.87–0.90 V and can result in accelerated degradation [77–83]. When delivering 10 kW DC power to the grid, average single cell potential calculated from the total FC stack voltage is in the range of 0.75–0.84 V, based on the total number of 434 cells [84]. Although average calculated cell potential is lower than 0.87 V, cell potentials of individual cells can differ from the calculated average and possibly face higher potentials. Extended periods at high cell potentials resulting into accelerated degradation, can be reduced by smart hybridization between HV battery and FC [78, 85], especially if the V2G power production profile is known upfront it could be incorporated in the power management. The influence of the V2G power production on the degradation of the FC is still a relatively uncovered topic in literature.

The mean $\eta_{T2G\text{-}AC}$ of 43% (51% on an LHV basis) gives a specific electricity production of 17 kWh kg^{-1} H_2. With current hydrogen prices of 10–14 \$ kg^{-1} at hydrogen fueling stations in California [86, 87] and 9.5 € kg^{-1} in Germany [88], this would result in an V2G electricity price of 590–825 \$ MWh^{-1} and 560 € MWh^{-1}, respectively, when considering the price of dispensed hydrogen only. Hydrogen fueling infrastructure is still at a development stage, so the cost of hydrogen fuel for fuel cell powered road transport is not yet comparable to conventional transportation fuels [88]. The current hydrogen prices are initial, politically motivated prices jointly determined by the project partners [88]. There is a high potential of lower hydrogen prices at fueling stations with economies of scale [89–92], i.e., when the number of FCEVs (including vans, buses and trucks) increase, hydrogen production and refueling infrastructure costs decrease and result in a dispensed hydrogen price of 2–4 € kg^{-1} [90–94]. Combined with a future expected maximum FC system efficiencies of 60% (70% on an LHV basis) [59, 95] and similar $\eta_{T2G\text{-}AC}$ or $\eta_{T2G\text{-}DC}$, V2G electricity price would become 85–170 € MWh^{-1}, when considering the price of dispensed hydrogen only.

In the period of 2015–2017 in the Californian electricity market, the 5-minute and 15-minute positive imbalance prices rose above 250 \$ MWh^{-1} for respectively 0.9% and 0.3% of the year, with some periods above 1,000 \$ MWh^{-1} [96, 97]. In 2017 in the German electricity market, imbalance prices above 85, 170, 250 and 560 € MWh^{-1} occurred respectively for 8.8 %, 0.9 %, 0.3 % and 0.1 % of the year [98, 99]. Future business models for FCEV2Gs participating in electricity imbalance markets rely on future FC system efficiency, imbalance and hydrogen prices. Other relevant business model parameters need additional research; for example the future costs of V2G infrastructure, FC systems and FC system additional degradation, operation and maintenance due to the V2G load cycles.

3.5 Hydrogen Consumption in Spinning Reserve Mode

Table 3 shows the hydrogen consumption in the "spinning reserve" (or idling mode) tests. Tests conducted for varying durations on different dates throughout the year revealed a relatively constant hydrogen consumption rate of approximately 0.040 kg h^{-1}. Taking the 5 kg hydrogen mass available for V2G purposes mentioned in Section 3.4, the maximum running time in spinning reserve mode is projected to be 125 h – a little over five days. A hydrogen consumption rate of 0.040 kg h^{-1} corresponds to an average hydrogen power flow of 1.6 kW (on an HHV basis). At an estimated FC stack gross efficiency of 40%, approximately 0.6 kW electrical power is produced to power the FCEV's auxiliary devices. This long-term idling power consumption could possibly be reduced in a purpose-built V2G FCEV.

During the "spinning reserve" tests, the FCEV is in idling mode and the HV battery and FC are only powering the FC auxiliary components and instruments, see Section 2.6. Because the FC power production is low, so is the water production. High calculated average FC stack air stoichiometry values above 10 occur for more than 70% of the time during the "spinning reserve" tests. This could result in a high removal rate of produced water, low humidification of the membrane and therefore higher probability of accelerated degradation [75]. Additional research focused on the conditions at individual cells could provide more insight into the effects of prolonged "spinning reserve" operation on the rate of degradation.

Cell potentials higher than 0.87 V and up to 1.5 V can cause accelerated degradation and are associated with operating conditions, such as idling, no load, prolonged periods of no use, start-up and shutdown [78, 82]. For an FCEV not used for V2G purposes (driving only) and depending on the usage profile, idling time at cell potentials of approximately 0.9 V could amount up to 1,000 h over a vehicle's 5,500 h of operational life [100]. Time spent at open circuit voltage (OCV) of approximately 0.95 V during no load conditions could be over 100 h [100]. Yu et al. show there is a significant lower durability for an equal number of hours spent at OCV than at idle conditions

Table 3 Results from ''spinning reserve'' tests.

#	Date / DD-MM-YY	t_{test} / h:mm	Δm_{H_2} / kg	$\Delta m\ \Delta t^{-1}$ / kg h^{-1}
1	19-01-16	11:02	0.52	0.047
2	07-04-16	09:00	0.39	0.043
3	08-04-16	09:03	0.37	0.041
4	21-07-16	10:00	0.39	0.039
5	25-07-16	09:14	0.35	0.037
6	27-07-16	46:30	1.76	0.038
7	01-08-16	45:28	1.59	0.035
8	03-08-16	49:03	2.04	0.041
Mean			0.92	0.040
Sample standard deviation			0.73	0.004

[101]. For 25% of the time spent during the "spinning reserve" tests, the average calculated cell potential from the total FC stack voltage was higher than 0.87 V and could cause accelerated degradation. The impact of extended periods of time at high potentials during the "spinning reserve" tests and their impact on degradation need to be investigated further. Also smarter hybridization between HV battery and FC and V2G operation integrated in a flexible power management can possibly reduce operating time at high potentials [78, 85].

Apart from taking part in the imbalance market as described in Section 3.4, Poorte et al. show that FCEV2Gs are able take part in the frequency containment reserves (FCR) and automatic frequency restoration reserves (aFRR) markets [102]. E.g., hundred FCEV2Gs each providing 10 kW V2G power would represent 1 MW and have a hydrogen consumption rate of 4 kg h^{-1}. With the current hydrogen prices of 10–14 \$ kg^{-1} at hydrogen fueling stations in California [86, 87] and 9.5 € kg^{-1} in Germany [88], this would result in an "spinning reserve" fuel price of respectively 40–56 \$ MW^{-1} h^{-1} and 38 € MW^{-1} h^{-1}, when considering the price of dispensed hydrogen only. Annual mean prices of ancillary services markets in 2014 in the United States of America range from 1–40 \$ MW^{-1} h^{-1} [103] and FCR and aFRR prices in 2017 in Germany range from 1–23 € MW^{-1} h^{-1} [98].

Future business models for FCEV2Gs participating in FCR and aFRR imbalance markets rely on future FC system efficiency, FCR, aFRR and hydrogen prices. Other relevant business model parameters need additional research. For example the future costs of V2G infrastructure, FC systems and FC system additional degradation, operation and maintenance due to the V2G load cycles.

4 Conclusions

We performed a series of V2G tests in which a modified commercially available FCEV delivered 9.5 kW of AC power to the grid. This paper is the first to report the performance results of this kind of system. Our results show that the FCEV can be used for mobility and to generate power when parked. We contend that grid-connected FCEVs are indeed capable of meeting the requirements for future balancing power plants identified by Brauner et al. [2]. With a maximum V2G DC power output of 10 kW, the maximum downward and upward power gradients of the FC were –47 kW s^{-1} (–470 % s^{-1}) and +73 kW s^{-1} (+730 % s^{-1}) respectively, at the sample frequency of 5 Hz. The maximum downward and upward power gradients of the HV battery were –76 kW s^{-1} (–760 % s^{-1}) and +43 kW s^{-1} (+430 % s^{-1}), respectively, at the sample frequency of 5 Hz. Thus, the FC and HV battery in the FCEV have the ability to perform high power gradients (≥ 0.05 % s^{-1} of all power plants in the electricity grid combined). Also the FC and HV battery in the FCEV respond faster than conventional fast-reacting thermal power plants, which have maximum values of 1.67 % s^{-1} for hot starts [24–27]. Increasing the ability to perform high power gradients reduces the number of power plants in hot standby. Virtual power plants [47, 48] composed of many grid-connected FCEVs do indeed have this ability.

We have demonstrated that the FC in the FCEV have the ability to efficiently operate at 10–15 % of its total generation capacity in V2G mode. Whereas existing thermal power plants often can be operated at a low minimal generation of 40 %. If all cars were capable of delivering 100 kW (the same as when in driving mode) to the grid *via* a virtual power plant arrangement, 15–20 % minimal generation could be achieved without any problem. Tests at different DC powers in the range of 0–10 kW done with the same set-up, show that 10 kW gives the highest V2G efficiency [72]. Conducting further tests at DC powers above 10 kW would provide full insight into the partial load and optimum V2G efficiency.

The grid-connected FCEV has an AC electric power efficiency of 43% on a HHV basis (51% on an LHV basis) when feeding 9.5 kW AC power to the electricity grid. This corresponds to a low partial load of 11-15% of the maximum FC DC power of 100 kW. The measured AC efficiency is close to the reported FC system DC efficiency of 46.8% on a HHV basis by Hyundai Motor Company [68]. These high efficiencies at low partial load are higher than efficient gas engines under low partial loads, although hydrogen production efficiency is not considered here. The V2G power in this work was limited to 10 kW DC and is examined as 100% V2G output. In a virtual power plant composed of many grid-connected FCEVs, reducing V2G output for every FCEV from 10 kW to 5kW DC could also be avoided by switching more FCEVs off instead of running them at lower power. Further tests at different V2G powers will provide more insight into the partial load and optimum V2G efficiency.

Approximately 38,500 startup/shutdown cycles take place during the life of automotive FC systems. Up to several startup/shutdown cycles can occur during a day, due to driving usage of the FCEV. If the V2G usage would be combined with the driving usage, so either occur before or after driving usage, then the V2G usage would not result into additional startup/shutdown cycles. If FCEVs were never switched off and continuously used for either driving or providing V2G energy services, start-ups/shutdowns would be eliminated. Additional degradation due to V2G load cycles (less than 10% rated power) could possibly be compensated for by reducing start-up/shutdown cycles, in combination with smarter power management of both the FC and the HV battery. Furthermore, inductive discharging instead of conductive discharging (by cable) could possibly reduce any further grid connection time.

We did not investigate the ability to schedule cars for this paper. However, the prospect of self-driving, cloud- and grid-connected cars [104, 105] with inductive charging and discharging [62–64] technologies in the future could facilitate scheduling of cars when faced with an insecure day ahead prognosis. Data pertaining to car parking locations, parking durations and tank fuel levels for a large number of cars, in combination with local grid imbalance data, could throw light on the problem of scheduling cars.

Acknowledgements

This work was financially supported by the Netherlands Organisation for Scientific Research (NWO) [Program "Uncertainty Reduction in Smart Energy Systems (URSES)", Project number 408-13-001] and GasTerra B.V.

C. B. Robledo and A.J.M. van Wijk would also like to acknowledge the CESEPS project, which has received funding from the EU Horizon 2020 research and innovation program under the ERA-Net Smart Grids plus grant agreement No. 646039, from the NWO and from BMVIT/BMWFW under the Energy der Zukunft program.

The authors would like to thank the following companies for their assistance with modifying the FCEV, building the V2G connection, installing the data logger and providing additional specifications for the FCEV: Hyundai Motor Company, Hyundai Motor Europe, Hyundai Motor Netherlands, Oriental Precision Industry, RDW, Accenda, HAN University of Applied Sciences, The Green Village – TU Delft.

List of Abbreviations and Symbols

AC	Alternating Current
aFRR	automatic Frequency Restoration Reserves
BEV	Battery Electric Vehicle
BHDC	Bi-directional High-voltage DC-DC Converter
CAN	Controller Area Network
CSD	Cold Shut Down
Δm_{H_2}	Hydrogen Consumption / kg
$\Delta m_{H_2} \Delta t^{-1}$	Hydrogen Consumption Rate / kg h^{-1}
$\Delta P\ \Delta t^{-1}$	Upward or Downward Electric Power Gradient / kW s^{-1} or % s^{-1}
ΔSOC	Difference State of Charge High Voltage Battery / %
DD	Day
DC	Direct Current
η	Efficiency / %
η_{DCAC}	Direct Current to Alternating Current Efficiency /%
$\eta_{T2G\text{-}AC}$	Higher Heating Value Tank-to-Grid Alternating Current Efficiency / %
$\eta_{T2G\text{-}DC}$	Higher Heating Value Tank-to-Grid Direct Current Efficiency / %
E_{AC}	Alternating Current Electrical Energy / kWh
E_{DC}	Direct Current Electrical Energy / kWh
$E_{HV\ Bat,\ max}$	High Voltage Battery Maximum Electrical Energy / 0.95 kWh
EV	Electric Vehicle
FC	Fuel Cell
FCEV	Fuel Cell Electric Vehicle
FCEV2G	Fuel Cell Electric Vehicle to Grid
FCR	Frequency Containment Reserves H_2 Hydrogen
HHV	Higher Heating Value of Hydrogen / 39.41 kWh kg^{-1}
HV	High Voltage
HVJB	High Voltage Junction Box
$I_{component,gross}$	Gross Current of Component (Fuel Cell or High Voltage Battery) / A
LED	Light Emitting Diode
LHV	Lower Heating Value of Hydrogen / 33.3 kWh kg^{-1}
MM	Month
NEDC	New European Driving Cycle
OCV	Open Circuit Voltage
p	Pressure / Pa
$P_{component,e,gross}$	Gross Electric Power of Component (Fuel Cell or High Voltage Battery) / kW
$P_{V2G\ DC\ max}$	Maximum Vehicle to Grid Direct Current Electric Power / 10 kW
PEM	Proton Exchange Membrane
PEMFC	Proton Exchange Membrane Fuel Cell
PHEV	Plug-in Hybrid Electric Vehicle
ρ	Density / kg m^{-3}
RDW	Dutch National Vehicle and Driving License Registration Authority
RGB	Red-Blue-Green
SAE	Society of Automotive Engineers
SOC	State Of Charge High Voltage Battery / %
t_{end}	Test End Time / h
$t_{GC/D}$	Grid Connect/Disconnect Time / h
t_{grid}	Grid connection time / h
t_{start}	Test Start Time / h
t_{test}	Test Start Time / h
T	Temperature / °C
T2G	Tank-to-Grid
T2G-AC	Tank-to-Grid Alternating Current
T2G-DC	Tank-to-Grid Direct Current
$U_{component}$	Voltage of Component (Fuel Cell or High Voltage Battery) / V
V2G	Vehicle-to-Grid
V2G-DCAC	Vehicle-to-Grid Direct Current to Alternating Current
V2L	Vehicle-to-Load
V2H	Vehicle-to-Home
V_{tanks}	Volume Capacity Hydrogen Tanks / 0.144 m^3
YY	Year

References

[1] M. Stappel, A.-K. Gerlach, A. Scholz, C. Pape, *The European Power System in 2030: Flexibility Challenges and Integration Benefit*, Fraunhofer Institute for Wind Energy and Energy System Technology (IWES), **2015**.

[2] G. Brauner, S. Bofinger, U. Schwing, W. Magin, W. Glaunsinger, I. Pyc, F. Steinke, *Elektrotechnik und Informationstechnik* **2014**, *131*, 361.

[3] European Commission, *Energy Roadmap 2050. Communication from the Commission to the European Parliament, the*

Council, the European Economic and Social Committee and the Committee of the Regions, **2011**.
[4] European Commission, *EU Reference Scenario 2016-Energy, Transport and GHG Emissions Trends to 2050*, **2016**.
[5] Union of the Electricity Industry – EURELECTRIC, *Flexible Gas Markets for Variable Renewable Generation*, **2014**.
[6] D. Hach, S. Spinler, *Energy Econ.* **2016**, *53*, 270.
[7] J. Nitsch, T. Pregger, Y. Scholz, *Langfristszenarien und Strategien für den Ausbau der Erneuerbaren Energien in Deutschland bei Berücksichtigung der Entwicklung in Europa und Global*, Deutsches Zentrum Für Luft- Und Raumfahrt (DLR), Fraunhofer Institute for Wind Energy and Energy System Technology (IWES), **2012**.
[8] Energistyrelsen – Danish Energy Agency, *Background Data from Energiscenarier Frem Mod 2020, 2035 Og 2050*, **2014**.
[9] G. Pasaoglu, D. Fiorello, A. Martino, L. Zani, A. Zubaryeva, C. Thiel, *Driving and Parking Patterns of European Car Drivers – a Mobility Survey*, Joint Research Centre (JRC) – European Commission (EC), **2012**.
[10] W. Kempton, J. Tomić, *J. Power Sources* **2005**, *144*, 280.
[11] W. Kempton, J. Tomić, *J. Power Sources* **2005**, *144*, 268.
[12] A. J. M. van Wijk, L. A. Verhoef, *Our Car as Power Plant*, Ios Press, Amsterdam, The Netherlands, **2014**.
[13] ZVEI – German Electrical and Electronic Manufacturers' Association, "Voltage Classes for Electric Mobility," can be found under https://www.zvei.org/fileadmin/user_upload/Presse_und_Medien/Publikationen/2014/april/Voltage_Classes_for_Electric_Mobility/Voltage_Classes_for_Electric_Mobility.pdf, **2013**.
[14] Hyundai Motor Company, "Hyundai ix35 fuel cell highlights," can be found under www.hyundai.com/worldwide/en/eco/ix35-fuelcell/highlights, **2013**.
[15] Toyota Motor Corporation, "outline of the Mirai," can be found under http://newsroom.toyota.co.jp/en/download/13241306, **2014**.
[16] Honda Motor Co., "Honda begins sales of all-new clarity fuel cell – clarity fuel cell realizes the world's top-class cruising range among zero emission vehicles of approximately 750 km," can be found under http://world.honda.com/news/2016/4160310eng.html?fro, **2016**.
[17] X. Luo, J. Wang, M. Dooner, J. Clarke, *Appl. Energy* **2015**, *137*, 511.
[18] J. Michaelis, F. Genoese, M. Wietschel, *Fuel Cells* **2014**, *14*, 14, 517.
[19] Y. Rebours, D. Kirschen, *Univ. Manchester* **2005**.
[20] IEA, *Energy Technology Perspectives 2014: Harnessing Electricity's Potential*, **2014**.
[21] A. Fernandes, T. Woudstra, A. J. M. van Wijk, L. A. Verhoef, P. V. Aravind, *Appl. Energy* **2016**, *173*, 13.
[22] V. Oldenbroek, S. Wijtzes, A. van Wijk, K. Blok, in *2017 IEEE Green Energy Smart Syst. Conf.*, **2017**, pp. 1–6.
[23] V. Oldenbroek, L. A. Verhoef, A. J. M. van Wijk, *Int. J. Hydrogen Energy* **2017**, *42*, 8166.
[24] J. Klimstra, M. Hotakainen, *Smart Power Generation 4th*, Avain Publishers, Helsinki, Finland, **2011**.
[25] R. Grosshauser, "Power Engineering – Turbines vs. Reciprocating Engines," can be found under http://www.power-eng.com/articles/print/volume-120/issue-11/features/turbines-vs-reciprocating-engines.html, **2016**.
[26] Energistyrelsen – Danish Energy Agency, *Technology Data for Energy Plants – Generation of Electricity and District Heating, Energy Storage and Energy Carrier Generation and Conversion (Updated 2017)*, **2012**.
[27] Parsons Brinckerhoff, *Technical Assessment of the Operation of Coal & Gas Fired Plants*, **2014**.
[28] TU Delta the independent newspaper of TU Delft, "Hydrogen car as power backup," can be found under https://www.delta.tudelft.nl/article/hydrogen-car-power-backup, **2016**.
[29] "Honda worldwide technology picture book power exporter 9000," can be found under http://world.honda.com/powerproducts-technology/Power Exporter9000/, **2017**.
[30] "Engineering the Extreme Capability of the Colorado ZH2," can be found under www.gm.com/mol/m-2016-oct-1101-zh2.html, **2016**.
[31] International Energy Agency Hybrid & Electric Vehicle (IEA-HEV), "Task 28 "Home Grids and V2X Technologies,"" can be found under http://www.ieahev.org/tasks/home-grids-and-v2x-technologies-task-28/, **2017**.
[32] T. W. Lim, B. K. Ahn, *ECS Trans.* **2012**, *50*, 3.
[33] Hyundai Motor Company, *ix35 FCEV Emergency Response Guide* **2013**.
[34] Pacific Engineering Company, "High Voltage Fuse EVFP DC450V 60A Breaking Capacity 2000A," can be found under https://www.pecj.co.jp/fuse/files/PEC_Fuse_Catalogue_en.pdf, **2016**.
[35] Panasonic Corporation, **2017**.
[36] SAE International, "SAE Electric Vehicle and Plug in Hybrid Electric Vehicle Conductive Charge Coupler Standard J1772," can be found under https://saemobilus.sae.org/content/j1772_201710, **2017**.
[37] imc Meßsysteme GmbH, "imc BUSDAQ-2," can be found under http://www.imc-berlin.com/products/measurement-hardware/imc-busdaq/device-options/, **2016**.
[38] Ningbo Ginlong Technologies, "Three Phase Wind Grid Tie Inverter GCI-10K-W," can be found under http://www.ginlong.com/en/Wind_Products/GCI_10K_W.html, **2014**.
[39] B. W. Evans, "Arduino Programming Notebook – Arduino Playground," can be found under https://playground.arduino.cc/uploads/Main/arduino_notebook_v1-1.pdf, **2007**.
[40] R. Torquato, Q. Shi, W. Xu, W. Freitas, *IEEE Trans. Smart Grid* **2014**, *5*, 2766.

[41] H. Köpf, E. Wilkening, C. Klosinski, M. Kurrat, in *ICEC 2014; 27th Int. Conf. Electr. Contacts*, VDE VERLAG GMBH, Dresden, Germany, **2014**, pp. 126–131.

[42] A. Sugawara, T. Goso, T. Sato, S. Tada, K. Tanabe, in *2013 2nd Int. Conf. Electr. Power Equip. – Switch. Technol. ICEPE-ST 2013*, **2013**.

[43] M. E. V. Team, *Current* **2008**, 1.

[44] A. Smets, O. Isabella, K. Jager, R. A. C. M. M. van Swaaij, M. Zeman, *Solar Energy: The Physics and Engineering of Photovoltaic Conversion, Technologies and Systems*, UIT Cambridge, Cambridge, **2016**.

[45] E. W. Lemmon, M. L. Huber, M. O. McLinden, *Ref. Fluid Thermodyn. Transp. Prop. (REFPROP), Version 9.1*, **2013**.

[46] General Electric Power, "LM6000 Hybrid Electric Gas Turbine (Hybrid EGT)," can be found under https://www.gepower.com/services/gas-turbines/upgrades/hybrid-egt, **2017**.

[47] F. Mwasilu, J. J. Justo, E. K. Kim, T. D. Do, J. W. Jung, *Renew. Sustain. Energy Rev.* **2014**, *34*, 501.

[48] B. Jansen, C. Binding, O. Sundström, D. Gantenbein, *Smart Grid Commun. (SmartGridComm), 2010 First IEEE Int. Conf.* **2010**, 149–154.

[49] H. Ribberink, K. Darcovich, F. Pincet, *EVS28 Int. Electr. Veh. Symp. Exhib.* **2015**, pp. 1–11.

[50] J. D. K. Bishop, C. J. Axon, D. Bonilla, M. Tran, D. Banister, M. D. McCulloch, *Appl. Energy* **2013**, *111*, 206.

[51] L. Wang, B. Chen, *SAE Tech. Pap.* **2017**, *2017–March*, DOI: 10.4271/2017-01-1699.

[52] R. Barnitt, "Analysis of Battery Wear and V2G Benefits Using Real-World Drive Cycles and Ambient Data," can be found under https://energy.gov/sites/prod/files/2014/03/f10/vss044_barnitt_2011_p.pdf, **2011**.

[53] M. Petit, E. Prada, V. Sauvant-Moynot, *Appl. Energy* **2016**, *172*, 398.

[54] R. Gough, C. Dickerson, P. Rowley, C. Walsh, *Appl. Energy* **2017**, *192*, 12.

[55] P. T. Yu, W. Gu, J. Zhang, R. Makharia, F. T. Wagner, H. A. Gasteiger, in *Polym. Electrolyte Fuel Cell Durab.*, **2009**, pp. 29–53.

[56] F. A. De Bruijn, V. A. T. Dam, G. J. M. Janssen, *Fuel Cells* **2008**, *8*, 3.

[57] L. Dubau, L. Castanheira, F. Maillard, M. Chatenet, O. Lottin, G. Maranzana, J. Dillet, A. Lamibrac, J. C. Perrin, E. Moukheiber, A. ElKaddouri, G. De Moor, C. Bas, L. Flandin, N. Caqué, *Wiley Interdiscip. Rev. Energy Environ.* **2014**, *3*, 540.

[58] R. E. Silva, F. Harel, S. Jemeï, R. Gouriveau, D. Hissel, L. Boulon, K. Agbossou, *Fuel Cells* **2014**, *14*, 894.

[59] Fuel Cell Technologies Office (FCTO) – U. S. Department of Energy (DOE), *Multi-Year Research, Development, and Demonstration (MYRD&D) Plan – Section 3.4 Fuel Cells*, **2017**.

[60] S. H. Kim, "Development of Fuel Cell Electric Vehicle in Hyundai · Kia Motors," can be found under http://www.fch.europa.eu/sites/default/files/documents/ga2010/sae-hoon_kim.pdf, **2010**.

[61] P. Salman, E. Wallnöfer-Ogris, M. Sartory, A. Trattner, M. Klell, H. Müller, A.-O. Bernt, M. Martin, K. Schiefer, M. Limbrunner, J. Höflinger, P. Hofmann, *SAE Tech. Pap.* **2017**, *2017–March*, DOI: 10.4271/2017-01-1185

[62] J. Y. Lee, B. M. Han, *IEEE Trans. Power Electron.* **2015**, *30*, 1784.

[63] Y. Fang, S. Cao, Y. Xie, P. Wheeler, in *2016 IEEE 8th Int. Power Electron. Motion Control Conf. IPEMC-ECCE Asia 2016*, **2016**, pp. 2709–2713.

[64] K. Tachikawa, M. Kesler, O. Atasoy, in *SAE WCX World Congr. Exp.*, SAE International, **2018**.

[65] P. H. Kydd, J. R. Anstrom, P. D. Heitmann, K. J. Komara, M. E. Crouse, *IEEE Power Energy Technol. Syst. J.* **2016**, *3*, 81.

[66] U. Eberle, B. Müller, R. von Helmolt, *Energy Environ. Sci.* **2012**, *5*, 8780.

[67] National Renewable Energy Laboratory – U.S. Department of Energy, "Fuel Cell Electric Vehicle Evaluation," can be found under https://www.nrel.gov/docs/fy16osti/66760.pdf, **2016**.

[68] J. Kim, S. Kim, *IEEE Electrif. Mag.* **2018**, *6*, 48.

[69] D. L. Wood, *Impacting Rapid Hydrogen Fuel Cell Electric Vehicle (FCEV) Commercialization: System Cost Reduction and Subcomponent Performance Enhancement*, SAE International, **2016**.

[70] R. K. Ahluwalia, X. Wang, A. Rousseau, R. Kumar, *J. Power Sources* **2004**, *130*, 192.

[71] T. Yoshida, K. Kojima, *Electrochem. Soc. Interface* **2015**, *24*, 45.

[72] C. B. Robledo, V. Oldenbroek, F. Abbruzzese, A. J. M. van Wijk, *Appl. Energy* **2018**, *215*, DOI: 10.1016/j.apenergy.2018.02.038

[73] F. Marignetti, M. Minutillo, A. Perna, E. Jannelli, *IEEE Trans. Ind. Electron.* **2011**, *58*, 2420.

[74] A. Rabbani, M. Rokni, E. Hosseinzadeh, H. H. Mortensen, *Int. J. Green Energy* **2014**, *11*, 91.

[75] M. Heuer, P. A. Bernstein, M. Wenske, Z. A. Styczynski, *Energies* **2013**, *6*, 3841.

[76] A. Iranzo, P. Boillat, J. Biesdorf, A. Salva, *Energy* **2015**, *82*, 914.

[77] S. S. Kocha, in *Polymer Electrolyte Fuel Cells Degardation* (Eds: M. Mench, E. C. Kumbur, T. N. Veziroglu), Academic Press, Boston, USA, **2012**, pp. 89–214.

[78] F. N. Büchi, M. Inaba, T. J. Schmidt, *Polymer Electrolyte Fuel Cell Durability*, Springer, New York, **2009**.

[79] A. Iiyama, K. Shinohara, S. Iguchi, A. Daimaru, *Handb. Fuel Cells*, John Wiley & Sons, Chichester, United Kingdom, **2010**, pp. 3221–3231.

[80] P. Pei, H. Chen, *Appl. Energy* **2014**, *125*, 60.

[81] S. S. Kocha, in *Fuel Cells, Sel. Entries from Encycl. Sustain. Sci. Technol.* (Ed: K.-D. Kreuer), Springer, New York, USA, **2013**, pp. 473–518.

[82] F. Barbir, T. N. Veziroğlu, H. Wang, M. L. Perry, *PEM Fuel Cells*, Second Edition, Academic Press, Boston, USA, **2013**.

[83] H. Wang, H. Li, X.-Z. Yuan, *PEM Fuel Cell Failure Mode Analysis*, CRC Press, New York, USA, **2011**.
[84] J. Arboleda, in *Eur. Hydrog. Energy Conf.*, **2018**, p. 21.
[85] C. Hochgraf, in *Encycl. Electrochem. Power Sources* (Ed: J. Garche), Elsevier, Amsterdam, The Netherlands, **2009**, pp. 236–248.
[86] California Fuel Cell Partnership (CAFCP), "Cost to refill," **2015**.
[87] Air Products, "Air Products' California Fueling Stations Offering Hydrogen Below $10 Per Kilogram," **2017**.
[88] Clean Energy Partnership (CEP), "How much does hydrogen cost at filling stations? – FAQ," **2018**.
[89] M. Robinius, P. Kuckertz, D. Stolten, T. Grube, K. Syranidis, M. Reuß, P. Stenzel, J. Linßen, *Comparative Analysis of Infrastructures: Hydrogen Fueling and Electric Charging of Vehicles*, **2018**.
[90] T. Grube, M. Robinius, D. Stolten, in *Wasserst. und Brennstoffzelle Technol. und Marktperspektiven* (Eds: J. Töpler, J. Lehmann), Springer Berlin Heidelberg, Berlin, Heidelberg, Germany, **2017**, pp. 245–261.
[91] C. Chardonnet, L. De Vos, F. Genoese, G. Roig, F. Bart, T. Ha, B. Van Genabet, *Early Business Cases for H2 in Energy Storage and More Broadly Power to H2 Applications*, **2017**.
[92] Fuel Cell Technologies Office (FCTO) – U. S. Department of Energy (DOE), *Multi-Year Research, Development, and Demonstration (MYRD&D) Plan – Section 3.1 Hydrogen Production*, **2015**.
[93] M. Robinius, G. Erdmann, D. Stolten, *Strom- und Gasmarktdesign zur Versorgung des deutschen Straßenverkehrs mit Wasserstoff*, Forschungszentrum Jülich GmbH, Zentralbibliothek, Verlag, Germany, **2015**.
[94] U. Albrecht, M. Altmann, F. Barth, U. Bünger, D. Fraile, J.-C. Lanoix, E. Pschorr-Schoberer, W. Vanhoudt, W. Weindorf, M. Zerta, W. Zittel, *Study on Hydrogen from Renewable Resources in the EU Final Report*, **2015**.
[95] International Energy Agency (IEA), *2015 Technology Roadmap: Hydrogen and Fuel Cells*, **2015**.
[96] E. Hildebrandt, K. Collins, R. Kurlinski, R. Avalos, A. Blanke, M. Castelhano, A. Deshmukh, J. Gregory, C. McCown, G. Murtaugh, S. Koppolu, P. O'Connor, H. Pihl, D. Robinson, A. Swadley, K. Westendorf, *2016 Annual Report on Market Issues and Performance*, **2017**.
[97] Department of Market Monitoring, *Q4 2017 Report on Market Issues and Performance*, **2018**.
[98] Tennet, *Market Review 2017 – Electricity Market Inshights*, **2018**.
[99] Amprion, "2017 Balancing group price – Balancing groups – Energy Market," **2018**.
[100] J. Zhang, R. N. Carter, P. T. Yu, W. Gu, F. T. Wagner, H. A. Gasteiger, in *Encycl. Electrochem. Power Sources* (Ed: J. Garche), Elsevier, Amsterdam, **2009**, pp. 626–638.
[101] P. T. Yu, W. Gu, J. Zhang, R. Makharia, F. T. Wagner, H. A. Gasteiger, in *Polym. Electrolyte Fuel Cell Durab.* (Eds: F. N. Büchi, M. Inaba, T. J. Schmidt), Springer, New York, NY, **2009**, pp. 29–53.
[102] M. Poorte, *Technical and Economic Feasibility Assessment of a Car Park as Power Plant Offering Frequency Reserves*, Delft University of Technology, **2017**.
[103] Z. Zhou, T. Levin, G. Conzelmann, *Survey of U.S. Ancillary Services Markets*, USA, **2016**.
[104] H. Khayyam, J. Abawajy, B. Javadi, A. Goscinski, A. Stojcevski, A. Bab-Hadiashar, *Appl. Energy* **2013**, *111*, 971.
[105] M. Gerla, E. K. Lee, G. Pau, U. Lee, in *2014 IEEE World Forum Internet Things, WF-IoT 2014*, **2014**, pp. 241–246.